Pore shapes, volume distribution and orientations in monodisperse granular assemblies

Citation: Sufian, Adnan, Adrian R. Russell, Andrew J. Whittle, and Mohammad Saadatfar. "Pore Shapes, Volume Distribution and Orientations in Monodisperse Granular Assemblies." Granular Matter 17, no. 6 (September 5, 2015): 727–742.

As Published: http://dx.doi.org/10.1007/s10035-015-0590-0

Publisher: Springer-Verlag

Persistent URL: http://hdl.handle.net/1721.1/102386

Version: Original manuscript: author's manuscript prior to formal peer review

Pore shapes, volume distribution and orientations in monodisperse granular assemblies

Adnan Sufian[a], Adrian R. Russell[a,*], Andrew J. Whittle[b], Mohammad Sadaatfar[c]

[a] *School of Civil and Environmental Engineering, University of New South Wales, Sydney, New South Wales 2052, Australia*
[b] *Department of Civil and Environmental Engineering, Massachusetts Institute of Technology, Cambridge, Massachusetts 02139, United States of America*
[c] *Department of Applied Mathematics, Research School of Physics and Engineering, The Australian National University, Canberra ACT 0200, Australia*

Abstract

The complex mechanical behaviour of granular materials is commonly studied by considering the evolving particle contact network. An often overlooked feature is the influence of micro-scale geometric configuration of pores on the macroscopic response. This paper presents a series of tools to quantify the shape, volume distribution and orientation characteristics of the pore space. The proposed approach is validated using data from physical and numerical experiments with monodisperse assemblies of spheres. Individual pores are represented by polyhedral pore unit cells obtained by combining the Delaunay tessellation with an algorithm for merging Delaunay cells based on the concept of maximal inscribed sphere, after Al-Raoush et al. (2003). A pore shape parameter is proposed that relates pore volume and surface area, and is analytically related to the void ratio and the number of edges forming the polyhedral pore unit cell. The pore volume distribution is shown to be uniquely described by the analytical k-gamma distribution proposed by Aste and Di Matteo (2008). A pore orientation tensor is introduced to define the principal orientation of individual pore units. This is subsequently used to define a global orientation tensor that reveals an isotropic pore network for the reference monodisperse assemblies. The global orientation tensor is analytically expressed in terms of the parameters defining the pore volume distribution. The pore characteristics described in this paper provide the basis for describing the evolution of the pore space during deformation and its relationship to mechanical properties.

Keywords:
granular material, voids and inclusions, pore characteristics

1. Introduction

Granular materials exhibit complex macroscopic response due to the various length scales and corresponding particle-continuum duality (Wood, 2004). The evolution of the particle contact network is often considered to describe the complex mechanical response of granular materials. Numerous studies have presented extensive characterisation of micro-scale features of the contact network, including the presence

*Corresponding author. Tel: +61 2 9385 5035 Fax: +61 2 9385 6139
Email addresses: a.sufian@student.unsw.edu.au (Adnan Sufian), a.russell@unsw.edu.au (Adrian R. Russell), ajwhittl@mit.edu (Andrew J. Whittle), mos110@physics.anu.edu.au (Mohammad Sadaatfar)

of strong force chains aligned with the direction of major principal stress and supported against buckling by a network of weaker contacts, as well as evolving anisotropy of the contact network.

However, the influence of geometric pore characteristics on the macroscopic response of granular assemblies has received limited attention. In granular soils, the pore space is a complex interconnected network and is of significance in describing physical processes ranging from fluid flow to internal erosion and deformation. Durán et al. (2010) stated that deformation of pores and tangential displacement at contacts are the primary contributors to strain in granular assemblies. Shire et al. (2013) specifically considered pore constrictions to explore anisotropy in numerical simulation of elemental shear tests (in triaxial compression, plane strain and triaxial extension modes), where the orientation of pore constrictions was related to the force chain network.

Therefore characterising micro-scale features of the pore space is an essential step in gaining a more complete understanding of the deformation response in granular materials. Only a few studies have presented quantitative characterisations of pore features. Reboul et al. (2008) presented a statistical description of pore volumes and inscribed sphere volumes, by implementing the modified Delaunay tessellation introduced by Al-Raoush et al. (2003). Kang et al. (2013) extended the application of the modified Delaunay tessellation by considering the evolution of pore sizes in the numerical simulation of a direct shear test.

The first theoretical framework to understand volume distribution in granular media was proposed by Edwards and Oakeshott (1989). This framework is based on the application of classical statistical mechanics to granular systems, whereby volume plays the role of the thermodynamic quantity energy. Aste and Di Matteo (2008) utilised this framework to demonstrate that a unique distribution of Voronoi cell volumes can be described analytically by a modified gamma distribution function.

The concept of pore shape is somewhat obscure given the continuity of the pore space within granular media. In the current context, pore shape refers to the geometry of individual pores. Even for assemblies of spheres, the shapes of unit pores are highly irregular. Prior studies have described pore shape qualitatively (Graton and Fraser, 1935, Nolan and Kavanagh, 1994) or approximated the unit pore with simple geometric objects. Ordonez-Miranda and Alvarado-Gil (2012) described pores as spheroids with a defined aspect ratio, while Li and Li (2009) defined pore shape as the ratio of the half-radii of an ellipse approximation of unit pores in the 2D void cell system.

Further, assessing the orientation characteristics of the pore space is of importance in describing anisotropy in granular systems. The evolving contact network is typically expressed through orientation distribution functions given by spherical harmonics expansion (Chang and Yin, 2010, Radjai et al., 2012), or through the application of a fabric tensor (Oda and Iwashita, 1999). However, there has been limited application of these concepts to describe the orientation of pores. Konishi and Naruse (1988) presented a 2D void tensor allowing for the determination of the principal orientation of individual pores, which can subsequently be implemented in a mean void tensor to describe a collection of pores. A 3D fabric tensor is implemented in (Shire et al., 2013) to quantify stress-induced anisotropy by considering the orientation of pore constrictions.

This paper presents quantitative tools to describe shape, volume distribution and orientation characteristics of the pore space in granular assemblies. The modified Delaunay tessellation proposed by Al-Raoush et al. (2003) is implemented to provide a physically intuitive definition of unit pores. Pore shape is defined after Russell (2014) and can be related to the local void ratio and number of edges forming the polyhedral

Table 1: Datasets used for validation of pore characterisation

Dataset E-D			Dataset N-GL			Dataset N-RLP		
Assembly	N_{REV}	ϵ_{REV}	Assembly	N_{REV}	ϵ_{REV}	Assembly	N_{REV}	ϵ_{REV}
p1v	2353	0.6606	*m1g*	5116	0.8137	*m1l*	5111	0.564
p2v	2066	0.6528	*m2g*	5101	0.784	*m2l*	5116	0.564
p3v	2184	0.6683	*m3g*	5102	0.7406	*m3l*	5113	0.583
p4v	2347	0.6667	*m4g*	5101	0.698	*m4l*	5101	0.6563
p5v	2277	0.6838	*m5g*	5108	0.6833	*m5l*	5107	0.7887
p6v	2632	0.6787	*m6g*	5110	0.6689	*m6l*	5098	0.6979
p7v	1933	0.6709	*m7g*	5111	0.5782	*m7l*	5110	0.7338
p8v	1729	0.6556	*m8g*	5108	0.5756	*m8l*	5099	0.613
p9v	1821	0.6708	*m9g*	5093	0.5723	*m9l*	5103	0.7609
p10v	1936	0.6762	*m10g*	5099	0.5699	*m10l*	5129	0.6328
p11v	2028	0.6845				*m11l*	5101	0.81
p12v	2174	0.6801				*m12l*	5101	0.677
						m13l	5095	0.6043
						m14l	5099	0.8159
						m15l	5099	0.8175

unit pore. This paper also investigates the applicability of the analytical k-gamma distribution function proposed by Aste and Di Matteo (2008) to describe the pore volume distribution. Further, a novel pore orientation tensor is proposed, which is applicable at the micro-scale to define the orientation of individual pores and also at the macro-scale to explore anisotropy of the granular assembly.

The proposed approach to characterise pore shape, volume distribution and orientation is validated using data from physical and numerical experiments of monodisperse assemblies of spheres. The E-D dataset has been obtained from physical experiments and comprise disordered assemblies of hard, spherical, acrylic beads (with slight polydispersity of approximately 3%), formed by pouring the beads into a container, where the position of the particles have been determined through X-ray computed tomography (refer to Aste et al., 2005). The N-RLP and N-GL datasets have been developed by numerical simulations. These datasets were developed to investigate the random loose packing (N-RLP) and granular line (N-GL) boundary of the phase diagram for jammed matter in (Song et al., 2008)[1].

Each dataset comprises several assemblies and Table 1 summarises the number of particles in a Representative Element Volume, N_{REV}, and the corresponding void ratio, ϵ_{REV}. Void ratio (ϵ) is defined as the ratio of pore volume to solid volume, and is related to the packing density (ρ) by the expression $\rho = 1/(1+\epsilon)$. All assemblies considered in this study fall within the amorphous regime for packing of monodisperse spheres. It is assumed that all assemblies comprise rigid particles (with the assumption of small contact deformation) and the static assemblies are at mechanical equilibrium under self-weight.

2. Tessellation of Pore Space

Even in assemblies of monodisperse spheres the pore space is geometrically complex and almost entirely interconnected. Hence, a space tessellation is employed to define a unit cell. Several methods (Bagi, 1996,

[1]N-RLP and N-GL datasets available online at http://lisgi1.engr.ccny.cuny.edu/~makse/soft_data.html

Hihinashvili and Blumenfeld, 2010, Li and Li, 2009, Satake, 1997) have been proposed to tessellate the pore space. This study initially employs a Delaunay triangulation to partition the pore space into tetrahedral Delaunay cells. A *pore unit* is then defined as the unit cell formed by merging Delaunay cells, as detailed below.

The Delaunay tessellation has been frequently utilised in delineating the pore space (Durán et al., 2010, Gao et al., 2012, Kang et al., 2013, Reboul et al., 2008, 2010, Vincens et al., 2014, Yang et al., 2006) and results in tetrahedral cells, where the four vertices correspond to particle centres. However, the Delaunay tessellation can exhibit issues in regards to triangulation close to sample boundaries, resulting in the formation of degenerate simplexes (Durán et al., 2010, Reboul et al., 2008, Yang et al., 2006). In order to avoid boundary irregularities, a Representative Element Volume (REV) comprising a central region with dimensions of 80% of the original sample size is selected. A sub-sampling procedure is employed that only considers completely internal tetrahedrons and avoids creating planarity on the REV boundaries. This ensured that no tetrahedral units were discounted from the analyses. However, all datasets included a degenerate simplex involving four near coplanar particles forming a flat tetrahedron. These cases were found to merge with adjacent Delaunay cells to form larger pore units.

While the Delaunay tessellation is a useful method to delineate the pore space, Al-Raoush et al. (2003) identifies two key drawbacks; 1) the pore space is artificially sub-divided into too many elements, and 2) Delaunay cells contain four faces. These restrictions result in the loss of physical description of a unit pore, and do not allow for any generality in the interconnection between pores. In order to alleviate these issues, Al-Raoush et al. (2003) introduced the concept of merging Delaunay cells to form pore units, which are polyhedral cells and can have convex and concave geometries. Following Al-Raoush et al. (2003), merging is based on the identification of the maximal inscribed sphere contained within the pore space for each Delaunay cell. The inscribed sphere is tangent to the corresponding four particles forming the Delaunay cell and is readily determined analytically. However, a local optimisation is required where the inscribed sphere is not completely located within the pore space. The local optimisation procedure is outlined in Appendix A.

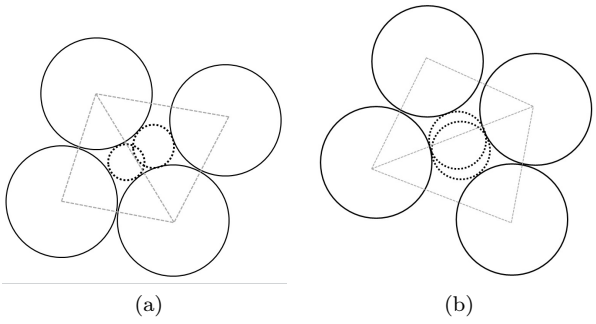

Figure 1: (a) Delaunay cells are merged if inscribed spheres overlap by any amount. (b) Delaunay cells are merged if the centre of the inscribed sphere is located within the reference inscribed sphere.

Two Delaunay cells are merged if the corresponding inscribed spheres overlap and this process is iterated for all Delaunay cells. However, the choice of the overlap criteria remains somewhat arbitrary. Two potential criteria are suggested in Al-Raoush et al. (2003) and Gao et al. (2012), which are illustrated in Figure 1. This

study employs the criterion shown in Figure 1a. While the choice of the overlap criteria will influence micro-scale features, it was found that this choice does not greatly influence the broader macroscopic characteristics discussed in this paper. It should be noted that an inscribed sphere can overlap multiple other inscribed spheres and this results in the formation of large pore units.

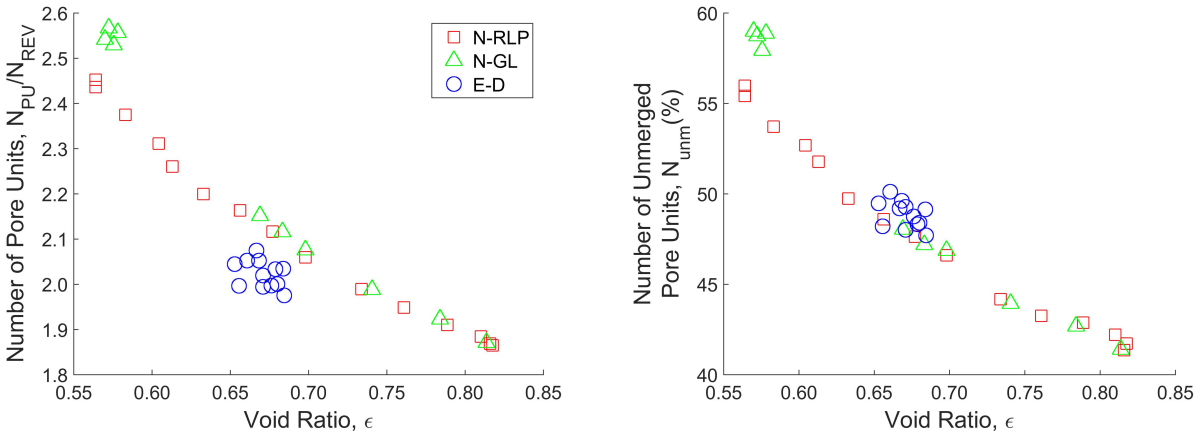

(a) (b)

Figure 2: (a) Variation in number of pore unit, N_{PU}, normalised by the number of particles within the REV, N_{REV}. (b) Variation in percentage of unmerged pore units, N_{unm} (%), that is tetrahedral pore units.

The polyhedral pore unit tessellation provides a better characterisation compared to the Delaunay tessellation. Figure 2a shows an increasing number of pore units with increasing density (that is, decreasing void ratio) for the datasets in Table 1. In dense assemblies, there is less probability in encountering large pore units containing many Delaunay cells. In fact, pore units in dense assemblies are more likely to be composed of only a few Delaunay cells, and this leads to an increase in the number of pore units with density. This is also reflected in the percentage of unmerged pore units, N_{unm} (%), in Figure 2b. This indicates that the percentage of tetrahedral pore units (that is, the smallest geometrically achievable pore unit) increases with density. Therefore, the pore unit tessellation characterises pores in a physically intuitive manner. This result is most clearly seen from the distribution of the number of Delaunay cells forming a pore unit (Figure 3). The behaviour is approximately exponential and agrees with the intuitive notion that there exist many small pores and fewer larger pores in a mechanically stable system.

3. Geometric Characteristics and Pore Shape

Tessellation of the pore space allows for the determination of geometric properties of individual Delaunay cells and pore units. There are three fundamental geometric properties of interest: volume of solids (V_s), volume of pores (V_p) and surface area of pores (S_p). All other geometric properties referred to in this paper are derived from these fundamental properties.

The volume of a tetrahedral Delaunay cell (V_{cell}) is readily calculated from the position vectors of the particles centres forming the Delaunay cell. The calculation of S_p takes into consideration the fact that surface area of pores and solids are the same, and is simply the sum of the surface areas of the parts of

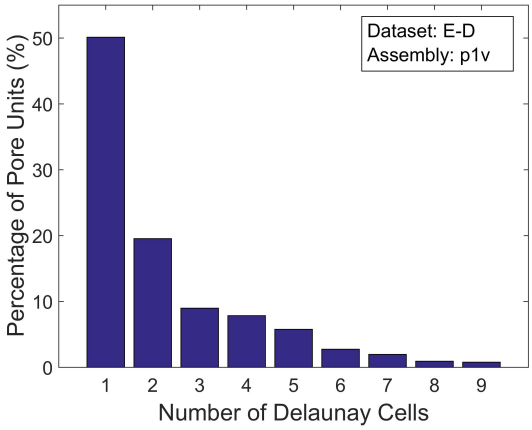

Figure 3: Distribution of the number of Delaunay cells forming a pore unit for a typical assembly.

the four particles contained within the tetrahedron (Figure 4). Each particle occupies a sector within the tetrahedron, whereby the sector is defined by the three vectors radiating from the centre of the particle. The surface area of this sector forms a spherical triangle, as shown in Figure 4b. The area of a spherical triangle corresponding to the i^{th} particle in the Delaunay cell is given by $S_{p,i} = r_{p,i}^2 \left(A + B + C - \pi\right)$, where $r_{p,i}$ is the radius of the i^{th} particle and A, B, C are the angles of the spherical triangle. A, B, C are calculated by considering the dihedral angles a, b, c in Figure 4b and applying spherical trigonometry. The total pore surface area is then simply $S_p = \sum_{i=1}^{4} S_{p,i}$. Further, each particle sector forms a pyramid with base given by the spherical triangle and hence the volume of each sector is given by $V_{s,i} = \frac{1}{3} S_{p,i} r_{p,i}$ and the total solid volume of the Delaunay cell is $V_s = \sum_{i=1}^{4} V_{s,i}$. The total pore volume in a Delaunay cell is simply $V_p = V_{cell} - V_s$.

The calculation of V_s, V_p and S_p for pore units is straightforward, as these properties are determined by simply summating the respective geometric property for each Delaunay cell forming the merged pore unit. This is an advantage of initially employing a Delaunay tessellation to the pore space.

Using the geometric properties calculated above, Russell (2014) introduced a novel pore shape parameter (F) to characterise the geometry of individual pore units. Suppose a pore unit has volume, $V_p = \Lambda_p d_p^3$, where Λ_p is a dimensionless pore volume parameter and d_p is the characteristic pore size. Similarly, a pore unit has a surface area defined by $S_p = \Gamma_p d_p^2$, where Γ_p is a dimensionless pore surface area parameter. The dimensionless shape parameter is then defined by Equation 1.

$$F = \frac{\Lambda_p}{\Gamma_p} \tag{1}$$

Russell (2014) suggests that for systems of equal sized spheres, the dimensionless shape parameter can be related to void ratio (ϵ) by Equation 2.

$$F = \frac{1}{6}\epsilon^{2/3} \tag{2}$$

This expression was derived by considering the unit cells presented in Graton and Fraser (1935). These unit cells considered only monodisperse particles and defined the unit cell in such a way that there is exactly

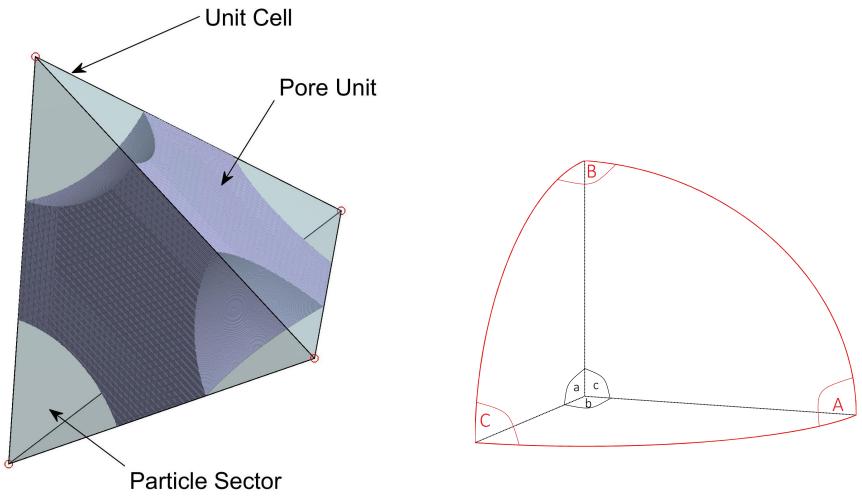

(a) (b)

Figure 4: (a) A tetrahedral unit cell with vertices defined by the particle centres. The geometry of the pore unit contained within the unit cell is shown, with all particle sectors removed. (b) Particle sector formed at each vertex of a Delaunay cell. The contribution to the surface area by a single particle is given by the spherical triangle with angles A, B, C.

one whole particle per cell. The expression in Equation 2 loses its generality for different definitions of a unit cell. Therefore, a generalised expression is developed relating F to void ratio for any definition of a pore unit cell for both monodisperse systems (Section 3.1) and polydisperse systems (Section 3.2).

3.1. Relationship for Monodisperse Particles

Consider the pore unit shown in Figure 4a. The pore volume is given by $V_p = \frac{\pi}{6} d_{eq}^3$, where d_{eq} is the diameter of the equivalent sphere with volume V_p. But pore volume is also defined as $V_p = \Lambda_p d_p^3$. By equating the two expressions (and taking $d_{eq} = d_p$), it can be shown that $\Lambda_p = \frac{\pi}{6}$. This relation is still applicable for polydisperse systems.

The surface area of particles, S_s, must be equal to the surface area of pores, S_p. The surface area of a sphere is given by πd_s^2. However, from Figure 4a, and depending on the method used to define a unit cell, exactly one sphere may not be contained within the unit cell. Hence, the surface area of particles within the unit cell is defined as $S_s = N_p \pi d_s^2$, where N_p is the equivalent number of spheres of diameter d_s that are included in the unit cell. As $S_s = S_p$ and using the definition $S_p = \Gamma_p d_p^2$, an expression for Γ_p is derived.

$$\Gamma_p = N_p \pi \left(\frac{d_s}{d_{eq}} \right)^2 \tag{3}$$

Using the definition of void ratio, $\epsilon = \frac{V_p}{V_s}$, it can be shown that:

$$\left(\frac{d_{eq}}{d_s} \right)^2 = (\epsilon N_p)^{2/3} \tag{4}$$

Substituting Equation 4 into Equation 3 gives:

$$\Gamma_p = \pi N_p^{1/3} \epsilon^{-2/3} \tag{5}$$

Therefore from Equation 5, the dimensionless shape parameter, F, can be defined as:

$$F = \frac{\Lambda_p}{\Gamma_p} = \frac{1}{6} N_p^{-1/3} \epsilon^{2/3} \tag{6}$$

which is independent of d_{eq}, d_p and d_s.

3.2. Relationship for Polydisperse Particles

The derivation can be extended to assemblies of polydisperse spheres. As above, $\Lambda_p = \frac{\pi}{6}$. In polydisperse assemblies, the surface area of particles is given by:

$$S_s = \sum_i \pi N_i d_i^2 \tag{7}$$

where d_i is the diameter of the i^{th} particle and N_i is the equivalent number of spheres of diameter d_i that are included within the unit cell. Note that Equation 7 does not place a limit on the number of particles forming a unit cell. This generality allows the expression to be used for either Delaunay cells or pore units. By equating $S_s = S_p$, an expression for Γ_p is derived:

$$\Gamma_p = \frac{\pi}{d_{eq}^2} \sum_i N_i d_i^2 \tag{8}$$

Using the definition of void ratio, it can be shown that the equivalent sphere diameter is:

$$d_{eq}^2 = \epsilon^{2/3} \left(\sum_i N_i d_i^3 \right)^{2/3} \tag{9}$$

By substituting Equation 9 into Equation 8, Γ_p for polydisperse assemblies is given by:

$$\Gamma_p = \frac{\pi \sum_i N_i d_i^2}{\epsilon^{2/3} \left(\sum_i N_i d_i^3 \right)^{2/3}} \tag{10}$$

Therefore, the pore shape parameter in polydisperse assemblies is given by:

$$F = \frac{\epsilon^{2/3}}{6} \cdot \frac{\left(\sum_i N_i d_i^3 \right)^{2/3}}{\sum_i N_i d_i^2} \tag{11}$$

It can be readily shown that Equation 11 simplifies to Equation 6 when d_i takes on the same value for all i (that is, for monodisperse assemblies).

3.3. Analytical Relationship between Shape Parameter and Geometry of Pore Units

Equations 6 and 11 suggest that the shape of pore units can be related to other geometric features. In this section, the pore shape parameter, F, is analytically related to void ratio, ϵ, and the number of edges forming the polyhedral pore unit, N_e, for assemblies of monodisperse spheres. In the following derivation, the pore unit is assumed to be a regular polyhedron and can be one of three platonic solids; tetrahedron ($N_e = 6$), octahedron ($N_e = 12$) and icosahedron ($N_e = 30$). All three platonic solids satisfy the condition that the Schläfli symbol, $p = 3$, that is, each face is composed of three edges. This is a reasonable assumption since pore units are unlikely to be composed of more than three edges as this would require two adjacent faces of merged Delaunay cells to be coplanar. In a highly disordered assembly this condition is unlikely to occur.

For a regular polyhedron, N_p is related to the solid angle, Ω, and the number of vertices of the polyhedron, N_v:

$$N_p = \frac{N_v \Omega}{4\pi} \tag{12}$$

From the Schläfli relationships for platonic solids, it is known that:

$$N_v = \frac{2N_e}{q} \tag{13}$$

where q is another Schläfli term defining the number of faces forming a vertex of the polyhedron. For platonic solids, the solid angle is:

$$\Omega = q\theta - \pi(q-2) \tag{14}$$

Combining Equation 13 and Equation 14 gives an expression for $N_v\Omega$, where θ is the dihedral angle.

$$N_v\Omega \quad = \quad 2N_e \left[\theta - \pi\left(\frac{q-2}{q}\right)\right] \tag{15}$$

q is determined by considering the following identity:

$$q = \frac{2N_e p}{2p + N_e p - 2N_e} \tag{16}$$

For the case $p = 3$, Equation 16 simplifies to $q = \frac{6N_e}{6+N_e}$, and a simplified expression for $\frac{q-2}{q}$ can be determined:

$$\frac{q-2}{q} = \frac{2}{3}\left(\frac{N_e - 3}{N_e}\right) \tag{17}$$

The dihedral angle for platonic solids is given by the solution to $\sin\left(\frac{\theta}{2}\right) = \cos\left(\frac{\pi}{q}\right) / \sin\left(\frac{\pi}{p}\right)$:

$$\theta \quad = \quad 2\sin^{-1}\left\{\frac{2\cos\left(\frac{\pi(6+N_e)}{6N_e}\right)}{\sqrt{3}}\right\} \tag{18}$$

Substituting Equation 17 and Equation 18 into Equation 15 provides an expression for N_p as a function of N_e, as shown in Equation 19.

$$N_p = \frac{N_v\Omega}{4\pi} = \frac{N_e}{2\pi}\left[2\sin^{-1}\left\{\frac{2\cos\left(\frac{\pi(6+N_e)}{6N_e}\right)}{\sqrt{3}}\right\} - \frac{2\pi}{3}\left(\frac{N_e-3}{N_e}\right)\right] \tag{19}$$

And F can be expressed as a function of N_e and ϵ:

$$F \quad = \quad \left(\frac{1}{6}\right)\left\{\frac{N_e}{2\pi}\left[2\sin^{-1}\left\{\frac{2\cos\left(\frac{\pi(6+N_e)}{6N_e}\right)}{\sqrt{3}}\right\} - \frac{2\pi}{3}\left(\frac{N_e-3}{N_e}\right)\right]\right\}^{-\frac{1}{3}}\epsilon^{\frac{2}{3}} \tag{20}$$

Figure 5 compares the analytical expression for F with the numerically derived values for a typical assembly. It is not surprising that the analytical solution for $N_e = 6$ and $N_e = 12$ describe the numerical data accurately, as the derivation is based on the tetrahedral and octahedral geometries. The analytical solution is interpolated for all other values of N_e and is a lower bound to the numerical data. Also, the numerical data for $N_e \geq 12$ form a relatively thick band, due to the presence of convex and concave polyhedrons with the same N_e values. As the derivation strictly considers regular convex polyhedrons, this explains why the analytical solution provides a lower bound approximation. Further, deviations from the analytical solution occur at high void ratios, as the assumption of regular polyhedral geometry becomes less accurate due to the highly irregular nature of large pores. Even so, Figure 5 demonstrates that the analytical solution in Equation 20 provides a very good fit for the vast majority of data.

4. Pore Volume Distribution

Characterising the pore volume distribution in granular assemblies is essential in quantifying the highly complex geometric configuration of pores. In this study, the distribution of pore unit volumes is described by the analytical k-gamma distribution function proposed by Aste and Di Matteo (2008).

$$f\left(V_p - V_{p,min} : k,\, \chi\right) = \frac{\left(V_p - V_{p,min}\right)^{k-1}}{\Gamma\left(k\right)\chi^k}e^{-\frac{V_p - V_{p,min}}{\chi}} \tag{21}$$

Equation 21 is a modified gamma distribution function in the variable $V_p - V_{p,min}$, with parameters k and χ, where $V_{p,min}$ is the theoretical minimum pore volume (for rigid particles). For Delaunay cells, $V_{p,min} = 0$ to account for the presence of flat tetrahedrons as discussed in Section 2. However, observations from the numerical analysis confirm that these degenerate Delaunay cells merge with adjacent tetrahedrons to form larger pore units. Consequently, the minimum pore volume for pore units is defined as the pore volume in a regular tetrahedron, where all edges contain contact points. This is given by Equation 22, where d_s is the particle diameter in a monodisperse assembly.

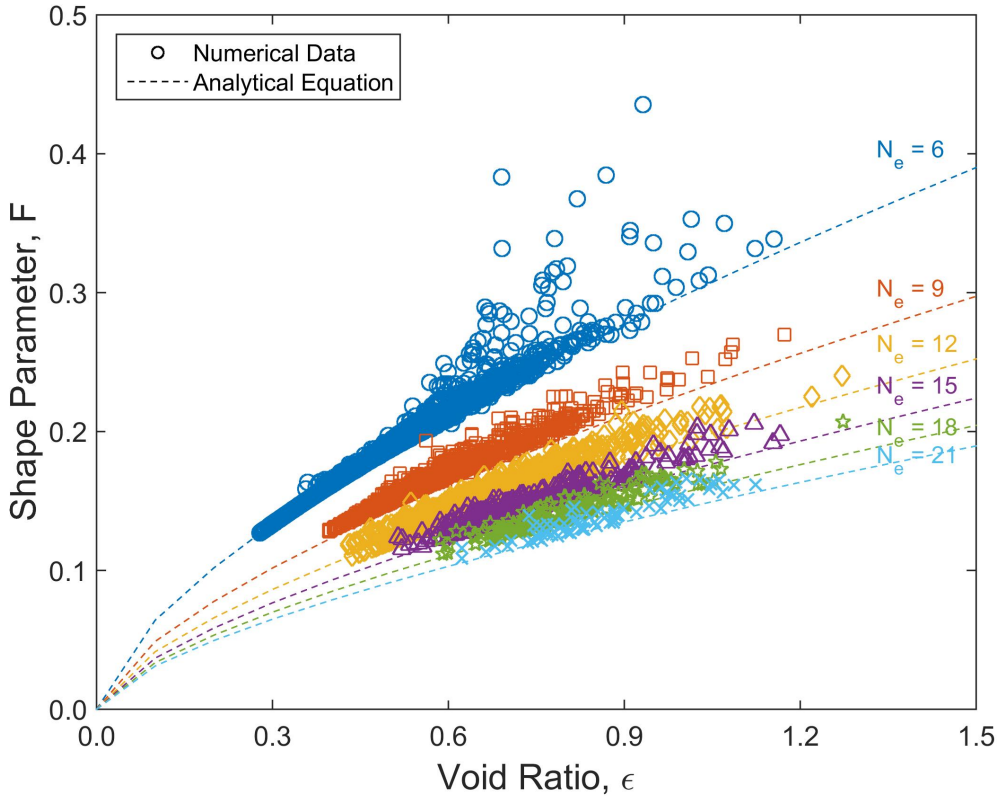

Figure 5: Comparison of the analytical expression in Equation 20 and the numerical data extracted from the *p1v* assembly of the E-D dataset.

$$V_{p,min} = \left(\frac{1}{6\sqrt{2}} - \frac{\arccos\left(\frac{23}{27}\right)}{6} \right) d_s^3 \approx 0.02597 d_s^3 \tag{22}$$

The parameter k can be determined analytically with consideration of fluctuations in pore volume $\left(\sigma^2\right)$:

$$k = \frac{\left(\langle V_p \rangle - V_{p,min}\right)^2}{\sigma^2} \tag{23}$$

where $\langle V_p \rangle$ is the mean pore volume and $\sigma^2 = \left\langle \left(V_p - V_{p,min}\right)^2 \right\rangle - \langle V_p - V_{p,min} \rangle^2$. The parameter χ can also be defined analytically by:

$$\chi = \frac{\langle V_p \rangle - V_{p,min}}{k} \tag{24}$$

While Aste and Di Matteo (2008) and Aste et al. (2007) validated the k-gamma distribution function by considering Voronoi cell volumes, Figure 6 demonstrates that the analytical k-gamma distribution function accurately reflects the distribution of pore unit volumes. However, there is a small discrepancy at very small pore volumes, $V_p - V_{p,min} \approx 0$, which was also noted in (Klatt and Torquato, 2014). The lack of an inflection point in the analytical solution shown in Figure 6 suggests that the most probable configuration

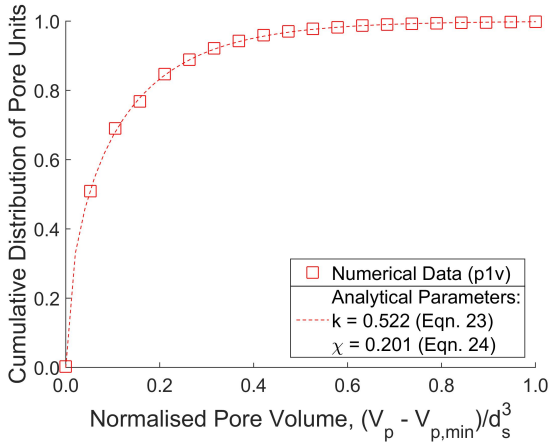

Figure 6: Distribution of pore unit volumes for the *p1v* assembly in the E-D dataset, where pore volume is normalised by d_s^3. The numerical data is compared against the analytical expression in Equation 21, where the parameter k is given by Equation 23 and the parameter χ is given by Equation 24.

occurs when $V_p - V_{p,min} = 0$, but this is not supported by the numerical analysis. While granular systems have a tendency to approach the densest possible local configuration (that is, the configuration of minimum potential energy), the phenomenon of geometric frustration (Francois et al., 2013) prevents the majority of pore units attaining the theoretical minimum pore volume in disordered assemblies of monodisperse spheres. This is also reflected in the observation of polytetrahedral structures in (Anikeenko and Medvedev, 2007), where it was demonstrated that there is a preference for the formation of irregular polytetrahedra comprising clusters of quasi-regular tetrahedrons that do not necessarily have the theoretical minimum pore volume. Hence, there is a lower limit above which the analytical expression in Equation 21 can provide an accurate approximation of the pore volume distribution.

Aside from this minor discrepancy, uniqueness in the pore volume distribution is observed when plotted in the variable $\frac{V_p - V_{p,min}}{\langle V_p \rangle - V_{p,min}}$, as shown in Figure 7. The collapsed distribution shown in Figure 7b can be fitted analytically by the parameter $k = 0.6$.

Aste and Di Matteo (2008) demonstrated that χ takes on physical meaning within the theoretical framework of granular statistical mechanics (proposed by Edwards and Oakeshott (1989)) as an equivalent granular temperature termed *compactivity* and reflects the macroscopic density of a static granular system (Hihinashvili and Blumenfeld, 2010). This is illustrated in Figure 8a which shows a linear relationship between χ and the macroscopic void ratio. The compactivity χ decreases with decreasing void ratio, which agrees with the intuitive notion that for denser systems, the number of accessible configurations reduces, that is, larger pores are less probable in dense assemblies. The results also show a cut-off at the random close packing limit ($\epsilon = 0.56$), which may signal the commencement of partial crystallisation within the assembly.

Equation 24 indicates that the quantity χk can be thought of as the mean free pore volume, $\langle V_p \rangle - V_{p,min}$, and reflects how far the granular system is from the densest possible configuration. However, it is important to note that the configuration corresponding to $\langle V_p \rangle - V_{p,min} = 0$ is not attainable, as this would require all pore units to be regular tetrahedrons and such a configuration cannot tile the pore space. Figure 8b shows there is also a linear relationship between χk and void ratio within the amorphous region with the mean free pore volume decreasing with decreasing void ratio.

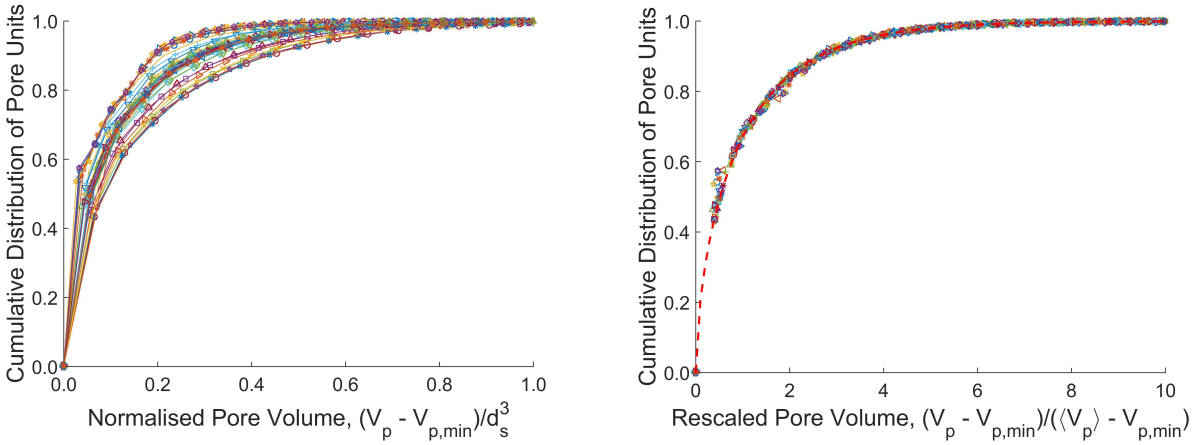

(a) (b)

Figure 7: (a) Cumulative distribution of normalised pore volume for all assemblies in Table 1. (b) Rescaled cumulative distribution plotted in the variable $(V_p - V_{p,min}) / (\langle V_p \rangle - V_{p,min})$ showing distribution collapsing on to a single curve.

The parameter k exhibits somewhat random fluctuations in a narrow range between 0.54 and 0.65, as illustrated in Figure 8c. According to Aste and Di Matteo (2008), k is an equivalent granular specific heat defined by $\frac{\partial \langle V_p \rangle}{\partial \chi}$. The linear relationship observed in Figure 8a suggests $\triangle\chi \propto \triangle\epsilon$, and similarly, the linear relationship shown in Figure 8b suggests $\triangle \langle V_p \rangle \propto \triangle\epsilon$. Hence, k is expected to be constant, where the observed fluctuations in Figure 8c may result from deviations from the respective linear relationships. Indeed, k was observed to fluctuate in a small region around $k \approx 12$ for Voronoi cell volume distribution in disordered assemblies (Aste and Di Matteo, 2008). This suggests that k is an indicator of the method of tessellation employed in partitioning the pore space.

5. Orientation Characteristics

The anisotropy of the pore network can be characterised by considering the orientation of pore units. An tensor ($\mathbb{P}$) is introduced to define the principal orientation of individual pore units. Following the definition of the fabric tensor (Oda and Iwashita, 1999), $\mathbb{P}$ is defined as:

$$\mathbb{P} = \frac{1}{N} \sum_{m=1}^{N} \mathbf{n}^m \otimes \mathbf{n}^m = \begin{bmatrix} P_{11} & P_{12} & P_{13} \\ P_{21} & P_{22} & P_{23} \\ P_{31} & P_{32} & P_{33} \end{bmatrix} \tag{25}$$

where N is the number of vectors. In order to describe orientation of pore units, $\mathbf{n}^m$ is defined as the vector normal to each triangular face of the polyhedral pore unit cell and is scaled by the square root of the area of the corresponding triangular face (a^m):

$$\mathbf{n}^m = \sqrt{a^m} \hat{\mathbf{n}}^m \tag{26}$$

where $\hat{\mathbf{n}}^m$ is the unit normal vector to the triangular face. $\mathbf{n}^m$ is therefore the projection of the surface area of each face to the corresponding coordinate axes. Components of the orientation tensor are given by:

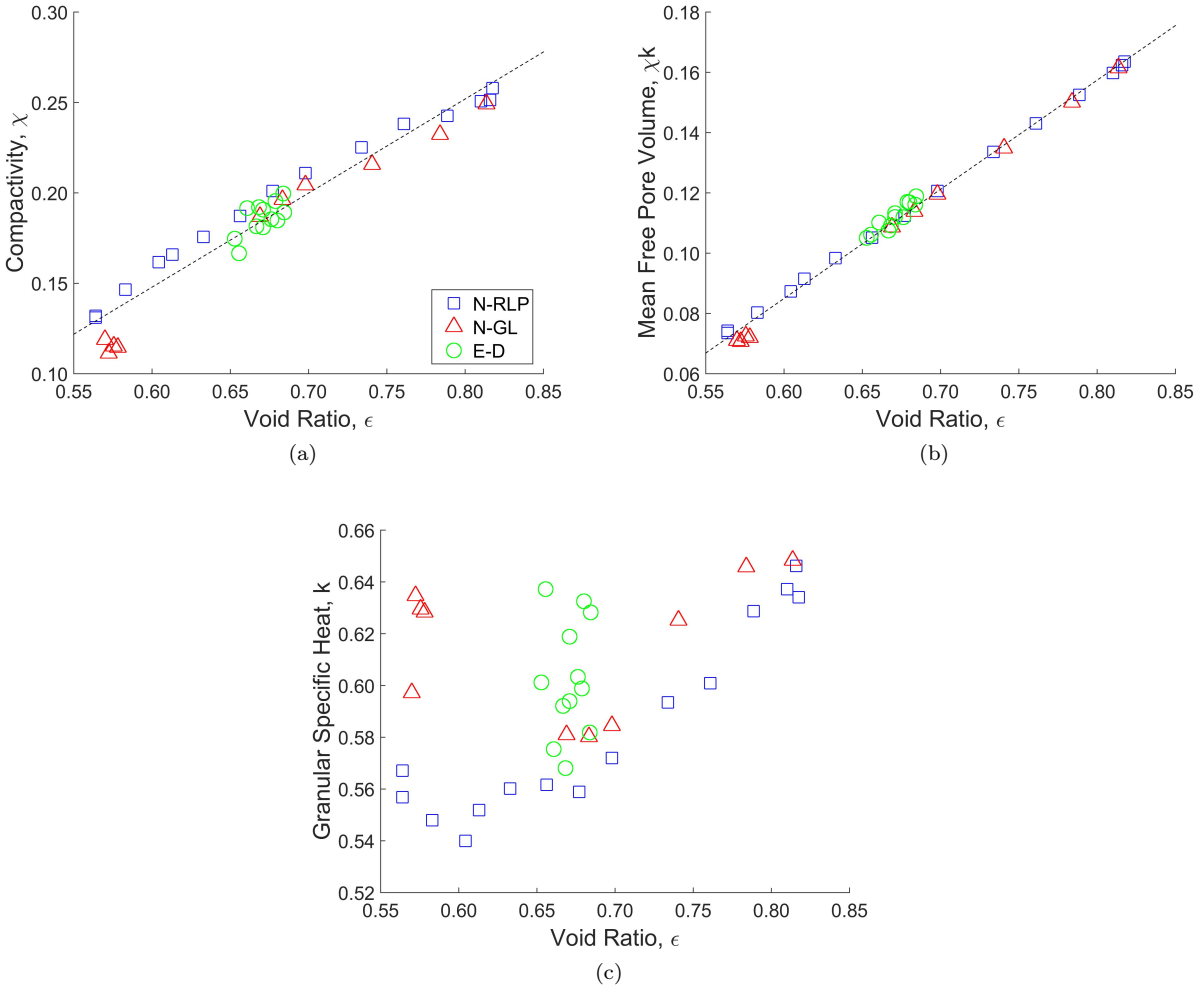

Figure 8: Variation in the parameters defining pore volume distribution for all assemblies in Table 1.

$$P_{ij} = \frac{1}{N} \sum_{m=1}^{N} a^m \hat{n}_i^m \hat{n}_j^m \tag{27}$$

$\mathbb{P}$ is a symmetric tensor and it can be readily shown that $\mathrm{tr}\,(\mathbb{P}) = \langle a^m \rangle$, that is, $\mathrm{tr}\,(\mathbb{P})$ is the average surface area per triangular face. Further, the non-diagonal terms reflect the skew or distortion of the surface area of a pore unit within a particular plane. Hence, it is easy to see that when the principal axes coincide with the coordinate system, $\mathbb{P}$ will only contain diagonal terms, as there will be no skew in the surface area. Hence, it is convenient to decompose the orientation tensor into isotropic and anisotropic components:

$$\mathbb{P} = \kappa \mathbb{I} + \kappa \mathbb{F} \tag{28}$$

where κ is a scalar quantity, $\mathbb{I}$ is the isotropic tensor given by the identity matrix and $\mathbb{F}$ is the anisotropic orientation tensor.

Taking the matrix inner product of Equation 28 with $\mathbb{I}$ and setting $\kappa\left(\mathbb{F}:\mathbb{I}\right)=0$, the result $\mathbb{P}:\mathbb{I}=\kappa\left(\mathbb{I}:\mathbb{I}\right)$ is obtained from which an expression for the scalar quantity κ can be explicitly defined:

$$\kappa=\frac{\mathrm{tr}(\mathbb{P})}{3}=\frac{\langle a^m\rangle}{3} \tag{29}$$

Further, setting $\kappa\left(\mathbb{F}:\mathbb{I}\right)=0$ places an additional constraint on the anisotropic orientation tensor; $\mathrm{tr}\left(\mathbb{F}\right)=0$. $\mathbb{F}$ is also a symmetric tensor and reflects the change in surface area of the polyhedral cell required to bring about isotropic orientation.

An eigen-decomposition of the orientation tensor results in an eigenvalue matrix ($\mathbb{D}$) and an eigenvector matrix ($\mathbb{V}$), which can be interpreted to provide the principal axes of orientation of individual pore units. The eigenvalues (λ) are determined from the solution to $f\left(\lambda\right)=\det\left(\mathbb{P}-\lambda\mathbb{I}\right)=0$. This reveals an interesting relationship that $\mathrm{tr}\left(\mathbb{D}\right)=\langle a^m\rangle$, which suggest that the eigenvalues reflect the average surface area per triangular face projected in the principal directions. Consequently, the major, minor and intermediate axes of orientation are defined by the minimum, maximum and intermediate eigenvalues in $\mathbb{D}$, respectively. Intuitively, the direction of maximum elongation corresponds to the minimum surface area projected in that direction, while the direction of minimum elongation corresponds to the maximum surface area. This approach to determining principal axes has been validated by comparison with a bounding ellipsoid approximation of pore units.

The formulation outlined above can be applied to define the major direction of orientation of all pore units forming an assembly. The vector defining the major direction of orientation can be expressed in terms of its azimuthal (ϕ) and elevation angle (β), or alternatively using the terminology of structural geology as the dip direction and dip angle, respectively. A lower hemisphere equal-area stereographic projection can be used to display the distribution of pore unit orientations. This analysis has been conducted for all assemblies in the E-D, N-RLP and N-GL datasets (Table 1). Figure 9a shows a typical stereonet using a probability density contour. The stereonet suggests radial symmetry in pore orientation distribution, which is confirmed by the distribution of azimuthal angles shown in the rose diagram in Figure 9b.

The distribution of elevation angles (β) for all assemblies in Table 1 is shown in Figure 10. All assemblies have similar distribution in elevation angle, and coupled with the radial symmetry shown in Figure 9 suggests that all assemblies have the same pore orientation distribution. Diambra et al. (2007) provided an expression for the cumulative distribution of orientation with an elevation angle within $\pm\beta$ from the horizontal under axisymmetric conditions (Equation 30).

$$P\left(\beta\right)=\frac{1}{2\overline{\rho}}\int_{-\beta}^{\beta}\rho\left(\alpha\right)\cos\left(\alpha\right)\mathrm{d}\alpha \tag{30}$$

$\rho\left(\alpha\right)$ is a generalised probability distribution function and reflects the concentration of pores with an elevation angle α above the horizontal. $\overline{\rho}$ represents the average concentration defined by $\overline{\rho}=\frac{1}{V_p}\int\rho\left(\alpha\right)\mathrm{d}V_p$. For isotropic distributions, $\rho\left(\alpha\right)=\overline{\rho}$, and hence $P\left(\beta\right)=\sin\left(\beta\right)$. This is compared to the numerical analysis (Figure 10), and it is clear that the pore network is isotropically orientated for all assemblies.

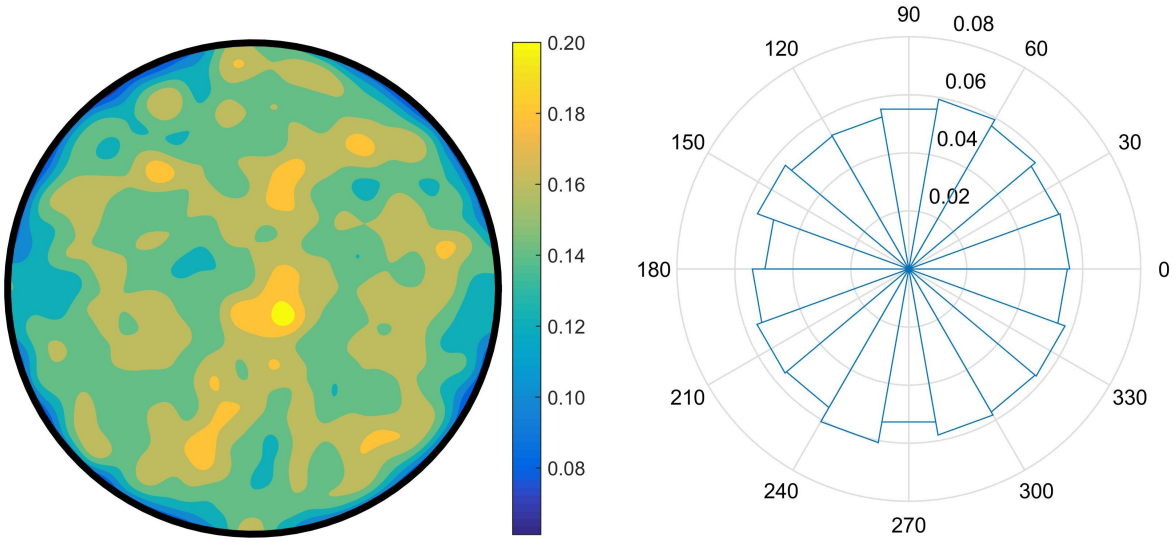

(a) (b)

$$\mathbb{P}^M = \begin{bmatrix} 0.0246 & 0.0000 & 0.0002 \\ 0.0000 & 0.0249 & 0.0004 \\ 0.0002 & 0.0004 & 0.0248 \end{bmatrix}$$

(c)

Figure 9: (a) Density contour stereonet of pore unit orientation for the *m1l* assembly in the N-RLP dataset. (b) The corresponding rose diagram for the *m1l* assembly reinforces the radial symmetry in the pore unit orientation distribution. (c) The global orientation tensor, $\mathbb{P}^M$, for the *m1l* assembly showing isotropic distribution of pores.

5.1. Global Orientation Tensor

Following (Konishi and Naruse, 1988), the principal orientation of individual pore units can be used to define a global orientation tensor $\left(\mathbb{P}^M\right)$, which determines the orientation characteristics for the set of pore units. For $\mathbb{P}^M$, $\mathbf{n}^m$ is defined as:

$$\mathbf{n}^m = \sqrt{V_p^m - V_{p,min}}\hat{\mathbf{n}}^m \tag{31}$$

where V_p^m is the normalised pore volume, $V_{p,min}$ is the normalised theoretical minimum pore volume and $\hat{\mathbf{n}}^m$ is the unit vector representing the major principal orientation of the pore unit (note that each pore unit comprises two complementary vectors). Using this definition, the elements of the $\mathbb{P}^M$ tensor are given by:

$$P_{ij}^M = \frac{1}{2N}\sum_{m=1}^{2N}\left(V_p^m - V_{p,min}\right)\hat{n}_i^m\hat{n}_j^m \tag{32}$$

Therefore, it is apparent from Equation 32 that $\mathbb{P}^M$ reflects the orientation distribution of pore volume in the sample, that is, what volume of the pore space is orientated in a given direction. Figure 9c shows a typical $\mathbb{P}^M$, which confirms the isotropic arrangement of pores, as the dominant terms of $\mathbb{P}^M$ are the leading diagonal elements, which are invariant to rotation of coordinate axis.

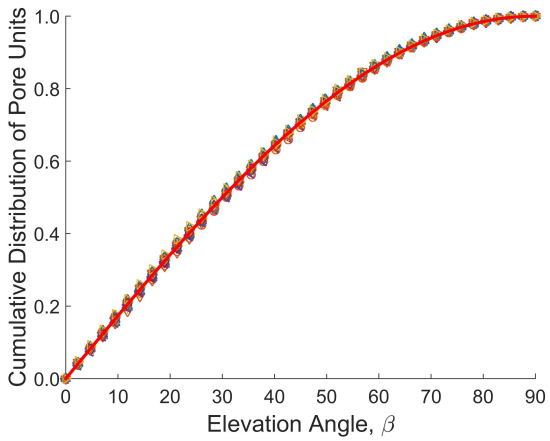

Figure 10: Cumulative probability distribution of elevation angle (β) for all assemblies. The analytical solution for isotropic orientation is also plotted.

Interestingly, analytical expressions for the elements of the $\mathbb{P}^M$ tensor can be derived with assumptions relevant to the datasets considered in this study. Note that the scaling factor in Equation 31 has been chosen in order to apply the pore volume distribution function in Equation 21. Suppose the distribution of vectors representing the major axis of orientation of pore units is defined by $E(\mathbf{n})$, which satisfies $\oint_\Omega E(\mathbf{n})\,\mathrm{d}\Omega = 1$, where Ω is the solid angle. If it is assumed that the volume of a pore unit is independent of its orientation, then Equation 32 can be expressed as:

$$P_{ij}^M = \int_{V_p} \widetilde{V_p} P\left(\widetilde{V_p}\right) \mathrm{d}\widetilde{V_p} \int_\Omega E(\mathbf{n})\,\hat{n}_i \hat{n}_j \mathrm{d}\Omega \tag{33}$$

where $\widetilde{V_p} = V_p^m - V_{p,min}$. This assumption is valid for the assemblies considered in this study due to the sample preparation process in both physical and numerical experiments. However, it is likely that there will be a relation between orientation and pore volume during shearing. The first term of the double integral in Equation 33 is the mean free pore volume, $\langle V_p \rangle - V_{p,min}$, which from Equation 24 is given by χk. Further, the isotropic arrangement demonstrated in Figure 9 and Figure 10 implies that $E(\mathbf{n}) = \frac{1}{\int_\Omega \mathrm{d}\Omega} = \frac{1}{4\pi}$. In spherical coordinates, a unit vector is given by $\hat{n} = \begin{pmatrix} \hat{n_1} \\ \hat{n_2} \\ \hat{n_3} \end{pmatrix} = \begin{pmatrix} \cos(\phi)\sin(\beta) \\ \sin(\phi)\sin(\beta) \\ \cos(\phi) \end{pmatrix}$ and the relationship $\mathrm{d}\Omega = \sin(\beta)\,\mathrm{d}\beta\mathrm{d}\phi$ holds. Therefore, Equation 33 can be alternatively expressed as:

$$P_{ij}^M = \frac{\chi k}{4\pi} \int_0^{2\pi} \int_0^{\pi} \hat{n}_i \hat{n}_j \sin(\beta)\,\mathrm{d}\beta\mathrm{d}\phi \tag{34}$$

Equation 34 can be easily solved and hence the analytical solution to $\mathbb{P}^M$ is given by:

$$\mathbb{P}^M = \frac{\chi k}{3}\mathbb{I} \tag{35}$$

Figure 11 demonstrates that the analytical solution in Equation 35 accurately reflects the numerically

determined global orientation tensor and confirms the isotropic orientation of the pore network.

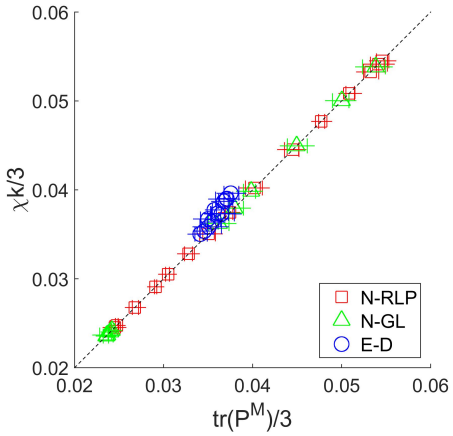

Figure 11: Comparison of the analytical expression in Equation 35 and the numerically determined global orientation tensor. The average of the diagonal elements in the numerically calculated $\mathbb{P}^M$, that is, $\frac{\mathrm{tr}(\mathbb{P}^M)}{3}$, is compared against the analytical value of $\frac{\chi k}{3}$. Perfect correspondence is shown by the dashed line (with slope 1 : 1). Further, the minimum and maximum diagonal elements in the numerically calculated $\mathbb{P}^M$ are shown by the + symbol to reflect the error between the numerical and analytical solution.

6. Conclusion

A set of parameters have been presented to quantify the micro-scale pore features in granular assemblies. The proposed approach has been validated with the use of data from physical and numerical experiments for monodisperse assemblies of spheres. Individual pore units were defined in a physically intuitive manner using the modified Delaunay tessellation proposed by Al-Raoush et al. (2003), which also readily allowed for the calculation of geometric properties of pore units.

Russell (2014) introduced a pore shape parameter (F) that related the volume and surface area of pores. Expressions were derived to relate F to void ratio for both monodisperse and polydisperse assemblies. For monodisperse assemblies, the derivation was extended to analytically show that pore shape can be related to void ratio and the number of edges forming the pore unit. This analytical solution agreed well with the numerically interpreted properties for all datasets.

The pore volume distribution was found to be uniquely defined by the analytical k-gamma distribution function, where χ corresponds to the compactivity and χk corresponds to the mean free pore volume. Both show a linear relationship with void ratio. The parameter k exhibited small random fluctuations around a constant value and is thought to provide an indication of the method of tessellation employed to partition the pore space. Even though this study considered pore space geometry and implemented a tessellation vastly different from Aste and Di Matteo (2008), the k-gamma distribution still remained applicable and was able to accurately describe pore volume distribution.

The principal orientation of individual pore units is defined by the orientation tensor, $\mathbb{P}$ (Equation 27). The distribution of the major principal orientation suggests that the pore network in all of the reference assemblies (Table 1) are isotropically orientated. The global orientation tensor, $\mathbb{P}^M$ (Equation 32), incorporated vectors defined by the major principal orientation of individual pore units scaled by the pore volume.

For assemblies of monodisperse spherical particles, an analytical expression for the global orientation tensor was derived in terms of the mean free pore volume (χk) and shown to agree well with values derived from physical and numerical experiments.

While this study explored micro-scale features in static granular assemblies, the long term goal of this research is to explore how these pore space features evolve under different load paths and whether the pore space can provide a better understanding of the complex mechanical response of granular soils.

Acknowledgements

A.S thanks A.J.W and Massachusetts Institute of Technology for hosting him since August 2014. A.R.R thanks M.S for hosting him during the first half of 2014 to start this work, and the University of New South Wales for granting him leave through the Special Studies Program. A.R.R also thanks the Australian Research Council for funding (DP150104123).

AppendixA. Local Optimisation to Inscribed Sphere

An iterative local optimisation procedure is required when the analytically determined inscribed sphere for a Delaunay cell (the *initial solution*) intersects adjacent particles, and is therefore not contained within the pore space. This is particularly prevalent for polydisperse assemblies and was only required for the E-D dataset in this paper. Particles intersected by the initial solution and those forming the Delaunay cell are referred to as *constraining particles* (Figure A.1a). For computational efficiency, only constraining particles located within two diametric shells from the reference Delaunay cell are considered in subsequent calculations. A combinatorics approach is implemented to define all possible configurations of four constraining particles. There are ${}^{n}C_{4}$ configurations, where n is the number of constraining particles and the inscribed sphere for each combination is determined (Figure A.1b). Only inscribed spheres that do not intersect the constraining particles are retained, where the largest retained inscribed sphere is the *maximal inscribed sphere* (Figure A.1c). If additional iterations are required (as is the case in Figure A.1c), additional constraining particles are considered and the combinatoric approach is implemented again to converge upon the maximal inscribed sphere located completely within the pore space. While this process does not completely disassociate the inscribed sphere from the Delaunay cell, it qualitatively produces the same results in Al-Raoush et al. (2003). It should be noted that while Figure A.1 illustrates a convex configuration, solution to non-convex configurations are non-trivial and require an additional tuning parameter that ensures that the inscribed sphere for each combination is within the boundary formed by the constraining particle.

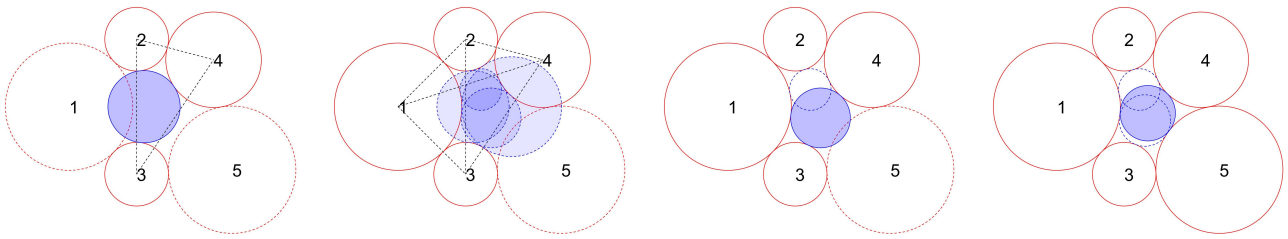

Figure A.1: A 2D local configuration of five polydisperse particles (comprising three Delaunay cells). (a) The inscribed sphere (the initial solution) to the Delaunay cell formed by particles 2, 3, 4 is shown to intersect particle 1, and consequently local optimisation must be undertaken. The constraining particles are 1, 2, 3, 4. (b) There are ${}^4C_3 = 4$ combinations and the inscribed sphere for each combination is illustrated. (c) Only two combinations have inscribed spheres that do not intersect the constraining particles. These solutions are retained and the largest of the retained solution is highlighted. Note that the highlighted inscribed sphere is still not completely within the pore space, as it intersects particle 5. Hence, a subsequent iteration is required with constraining particles 1, 2, 3, 4, 5. (d) The retained solutions for the subsequent iteration is shown and the maximal inscribed sphere contained completely within the pore space is highlighted. It is worth noting that the solution to the remaining two Delaunay cells also converges to the same local maxima.

References

Al-Raoush, R., Thompson, K., Willson, C. S., 2003. Comparison of Network Generation Techniques for Unconsolidated Porous Media. Soil Science Society of America Journal 67 (6), 1687–1700.

Anikeenko, A., Medvedev, N., Jun. 2007. Polytetrahedral Nature of the Dense Disordered Packings of Hard Spheres. Physical Review Letters 98 (23), 235504.

Aste, T., Di Matteo, T., Feb. 2008. Emergence of Gamma distributions in granular materials and packing models. Physical Review E 77 (2), 021309.

Aste, T., Matteo, T. D., Saadatfar, M., Senden, T. J., Schröter, M., Swinney, H. L., Jul. 2007. An invariant distribution in static granular media. Europhysics Letters (EPL) 79 (2), 24003.

Aste, T., Saadatfar, M., Senden, T., Jun. 2005. Geometrical structure of disordered sphere packings. Physical Review E 71 (6), 061302.

Bagi, K., 1996. Stress and strain in granular assemblies. Mechanics of Materials 22 (3), 165–177.

Chang, C. S., Yin, Z., 2010. Micromechanical Modeling for Inherent Anisotropy in Granular Materials. Journal of Engineering Mechanics 136 (7), 830–839.

Diambra, A., Muir Wood, D., Russell, A. R., Ibraim, E., Jan. 2007. Determination of fibre orientation distribution in reinforced sands. Géotechnique 57 (7), 623–628.

Durán, O., Kruyt, N. P., Luding, S., 2010. Micro-mechanical analysis of deformation characteristics of three-dimensional granular materials. International Journal of Solids and Structures 47 (17), 2234–2245.

Edwards, S. F., Oakeshott, R. B. S., 1989. Theory of Powders. Physica A 157 (3), 1080–1090.

Francois, N., Saadatfar, M., Cruikshank, R., Sheppard, A., Oct. 2013. Geometrical Frustration in Amorphous and Partially Crystallized Packings of Spheres. Physical Review Letters 111 (14), 148001.

Gao, S., Meegoda, J. N., Hu, L., 2012. Two methods for pore network of porous media. International Journal for Numerical and Analytical Methods in Geomechanics 36 (18), 1954–1970.

Graton, L. C., Fraser, H. J., 1935. Systematic packing of spheres - with particular relation to porosity and permeability. The Journal of Geology 43 (8), 785–909.

Hihinashvili, R., Blumenfeld, R., 2010. Structural Characterization of Porous and Granular Materials. In: Carrera, J. (Ed.), Proceedings of the XVIII International Conference on Water Resources. CIMNE, Barcelona, pp. 1–8.

Kang, D. H., Choo, J., Yun, T. S., Apr. 2013. Evolution of pore characteristics in the 3D numerical direct shear test. Computers and Geotechnics 49, 53–61.

Klatt, M. A., Torquato, S., Nov. 2014. Characterization of maximally random jammed sphere packings: Voronoi correlation functions. Physical Review E 90 (5), 052120.

Konishi, J., Naruse, F., 1988. A note on fabric in terms of voids. In: Satake, M., Jenkins, J. (Eds.), Micromechanics of Granular Materials: Proceedings of the U.S./Japan Seminar on the Micromechanics of Granular Materials. Elsevier Science Publishers B.V., Amsterdam, pp. 39–46.

Li, X., Li, X. S., 2009. Micro-Macro Quantification of the Internal Structure. Journal of Engineering Mechanics 135 (7), 641–656.

Nolan, G., Kavanagh, P., 1994. The size distribution of interstices in random packings of spheres. Powder Technology 78 (3), 231–238.

Oda, M., Iwashita, K., 1999. Mechanics of Granular Materials: An Introduction. A.A. Balkema, Rotherdam.

Ordonez-Miranda, J., Alvarado-Gil, J. J., Jun. 2012. Effect of the pore shape on the thermal conductivity of porous media. Journal of Materials Science 47 (18), 6733–6740.

Radjai, F., Delenne, J.-Y., Azéma, E., Roux, S., Mar. 2012. Fabric evolution and accessible geometrical states in granular materials. Granular Matter 14 (2), 259–264.

Reboul, N., Vincens, E., Cambou, B., 2008. A statistical analysis of void size distribution in a simulated narrowly graded packing of spheres. Granular Matter 10 (6), 457–468.

Reboul, N., Vincens, E., Cambou, B., 2010. A computational procedure to assess the distribution of constriction sizes for an assembly of spheres. Computers and Geotechnics 37 (1-2), 195–206.

Russell, A. R., 2014. How water retention in fractal soils depends on particle and pore sizes , shapes , volumes and surface areas. Géotechnique 64 (5), 379–390.

Satake, M., 1997. Three-dimension discrete mechanics of granular materials. In: Fleck, N., Cocks, A. C. F. (Eds.), lUTAM Symposium on Mechanics of Granular and Porous Materials. Vol. 2. Kluwer Academic Publishers, pp. 193–202.

Shire, T., O'Sullivan, C., Barreto, D., Gaudray, G., 2013. Quantifying stress-induced anisotropy using inter-void constrictions. Géotechnique 63 (1), 85–91.

Song, C., Wang, P., Makse, H., May 2008. A phase diagram for jammed matter. Nature 453 (7195), 629–32.

Vincens, E., Witt, K. J., Homberg, U., 2014. Approaches to determine the constriction size distribution for understanding filtration phenomena in granular materials. Acta Geotechnica (March).

Wood, D. M., 2004. Geotechnical Modelling. Taylor & Francis, Abingdon, UK.

Yang, R. Y., Zou, R. P., Yu, a. B., Choi, S. K., Jul. 2006. Pore structure of the packing of fine particles. Journal of Colloid and Interface Science 299 (2), 719–25.